JOURNAL OF GEOPHYSICAL RESEARCH, VOL. 104, NO. E8, PAGES 18,981–18,990, AUGUST 25, 1999

Lobate scarps and the Martian crustal dichotomy

Thomas R. Watters

Center for Earth and Planetary Studies, National Air and Space Museum
Smithsonian Institution, Washington, D.C.

Mark S. Robinson

Department of Geological Sciences, Northwestern University, Evanston, Illinois

Abstract. Landforms reflecting crustal shortening are found in the ancient highlands of the eastern hemisphere of Mars. These structures, referred to as lobate scarps, are interpreted to be thrust faults. Lobate scarps occur near and are oriented roughly parallel to the Martian crustal dichotomy, a major geologic and topographic boundary that divides the heavily cratered highlands from the relatively smooth, featureless northern lowlands. The long- and short-wavelength topography of lobate scarps in the northern Terra Cimmeria–Amenthes region have been analyzed using photoclinometry, Earth-based radar altimetry, and Mars Orbiter Laser Altimeter data. The measured relief of lobate scarps in this region ranges from ~110 to 1230 m, and they occur on gentle regional slopes that dip both toward and away from the dichotomy. Estimates of the horizontal shortening across the lobate scarps studied range from roughly 0.24 to 2.6 km ($n = 9$), assuming fault plane dips of 25°. The displacement-length (D-L) relationships of thrust faults associated with the lobate scarps are consistent with those observed for terrestrial fault populations. The compressional strain in the heavily cratered highlands near the dichotomy, determined using the D-L data for the lobate scarps, is estimated to be ~0.17%. Topographic data indicate that the dichotomy in the northern Terra Cimmeria–Amenthes region has a distinct topographic signature. The spatial and temporal relationship of the lobate scarps to the boundary suggests that they are related to its formation, supporting models for a tectonic origin of the crustal dichotomy.

1. Introduction

The highlands of Mars have landforms described as lobate scarps that are generally one-sided, are often lobate, and occur in linear or arcuate segments. They are morphologically similar to lobate scarps observed on Mercury [*Watters*, 1993; *Watters et al*., 1998]. The fact that many Martian and Mercurian lobate scarps clearly deform and offset crater floors and walls supports the interpretation that these structures are compressional tectonic features resulting from thrust faulting (Figures 1 and 2) [*Strom et al*., 1975; *Cordell and Strom*, 1977; *Melosh and McKinnon*, 1988; *Watters*, 1993; *Watters et al*., 1998].

Although the Tharsis dominated western hemisphere is the most prominent tectonic center on Mars, the eastern hemisphere has also experienced major tectonic events. Lobate scarps in highland materials of the eastern hemisphere record significant compressional deformation of some of the oldest terrain on Mars [see *Tanaka*, 1986] and account for ~18% of the total cumulative length of compressional structures on the planet [*Watters*, 1993]. Martian lobate scarps, like the analogous structures on Mercury, appear to occur on at least two different length scales, here described as moderate and large scale. Examples are found in the heavily cratered highlands of Amenthes and northern Terra Cimmeria (Figure 1). Amenthes Rupes (Figure 2) is one of the best preserved large-scale scarps on the planet. It exhibits greater relief and is longer than the moderate-scale scarps found in northern Terra Cimmeria (Figure 3). The lobate scarps in this region are about 300 to 400 km southwest of the Martian crustal dichotomy, a geologic boundary between the southern heavily cratered highlands and the relatively featureless northern lowlands. The orientations of the lobate scarps parallel that of the steep structural and/or erosional scarp that marks the crustal dichotomy (Figure 1). These lobate scarps are also radial to the Isidis basin, and it has been suggested that they are related to the formation of Isidis [*Wichman and Schultz*, 1989]. The close proximity and parallel orientation of the lobate scarps to the dichotomy boundary, however, strongly suggest that they may be related to the formation of the crustal dichotomy and may thus be significant in constraining models for its origin.

We present the results of a study of the short- and long-wavelength topography of lobate scarps in the northern Terra Cimmeria–Amenthes region through photoclinometric analyses, Earth-based radar altimetry, and Mars Orbiter Laser Altimeter (MOLA) data. A kinematic model for the formation of lobate scarps that involves thrust faults is used to estimate displacement and horizontal shortening. The displacement-length (D-L) relations of the faults associated with the lobate scarps is determined and compared to D-L data of terrestrial faults. The D-L data are also used to estimate the compressional strain recorded by the lobate scarps in the highlands near the dichotomy. Finally, the relationship between the lobate scarps in the northern Terra Cimmeria–Amenthes region and the origin of the crustal dichotomy is discussed.

Paper number 1998JE001007.
0148-0227/99/1998JE001007$09.00

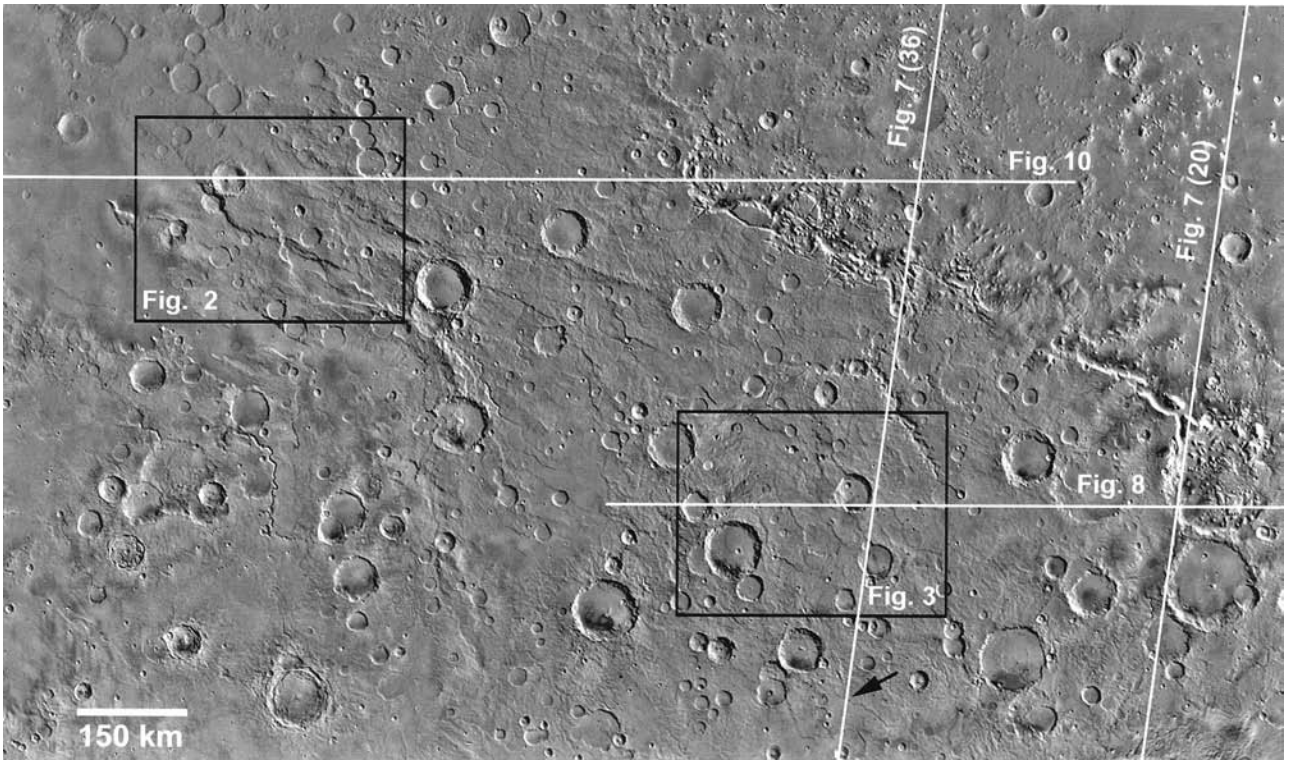

Figure 1. Viking Orbiter mosaic of the northern Terra Cimmeria–Amenthes region of Mars. The steep scarp that marks the Martian crustal dichotomy between the southern heavily cratered highlands from the northern lowlands strikes NW-SE (right side of mosaic). The black boxes indicate the locations of lobate scarps shown in Figures 2 and 3. The white lines indicate the locations of Mars Orbiter Laser Altimeter (MOLA) and Earth-based radar altimetry profiles shown in Figures 7, 8, and 10. The solid arrow indicates the location of the profile (lobate scarp H) shown in Figure 6. This mosaic was generated using images from *NASA* [1991].

2. Background

2.1. Mars Orbiter Laser Altimetry

Early results from MOLA, an instrument on the Mars Global Surveyor, have already greatly contributed to our knowledge of the detailed topography of Mars [*Smith et al*., 1998; *Zuber et al*., 1998]. MOLA determines the elevation of the surface within ~160-m footprints [*Zuber et al*., 1992]. The data have a maximum vertical resolution (precision) of ~30

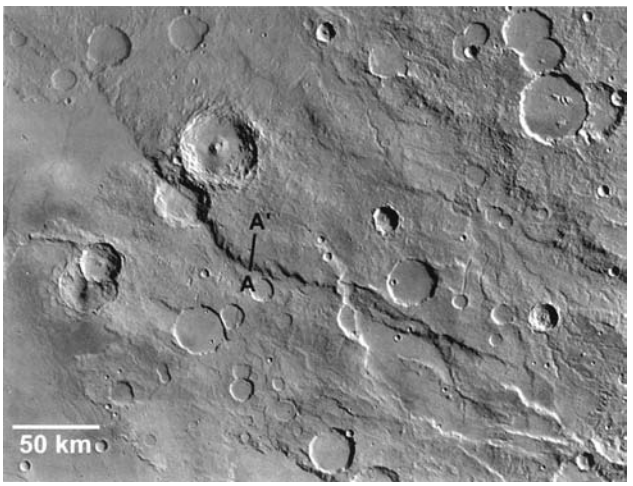

Figure 2. Viking Orbiter mosaic of Amenthes Rupes, possibly the largest thrust fault scarp on Mars, is over a kilometer high and over 400 km long. The line indicates the location of the photoclinometric profiles (A–A′) shown in Figure 9. The location of this mosaic is shown in Figure 1. This mosaic was generated using images from *NASA* [1991].

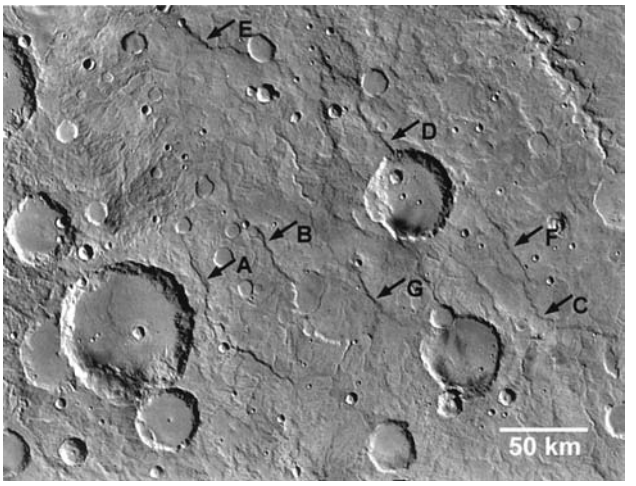

Figure 3. Viking Orbiter mosaic of a region in northern Terra Cimmeria. The area is dominated by a series of moderate-scale lobate scarps with orientations that roughly parallel the trend of the crustal dichotomy boundary. Arrows indicate the locations of photoclinometric profiles shown in Figure 4, and the location of this mosaic is shown in Figure 1. This mosaic was generated using images from *NASA* [1991].

cm, an absolute vertical accuracy of ~30 m, and along-track spatial resolution of 300 to 400 m [*Smith et al*., 1998]. The across-track shot spacing obtained during the nominal mapping mission will depend on the mapping orbit and will vary with latitude [see *Zuber et al*., 1992]. Two of the available tracks of data cross the northern Terra Cimmeria–Amenthes region (Figure 1) [see *Smith et al*., 1998, Figure 1; *Frey et al*., 1998].

2.2. Earth-Based Radar Altimetry

Another source of topography is Earth-based radar altimetry [*Roth et al*., 1980; *Downs et al*., 1982]. The elevation of a point on the surface is derived within a footprint that varies in dimension with the geometry of the observation. The footprints or resolution cells for Goldstone observations made during Mars oppositions that occurred between 1973 and 1982 [*Roth et al*., 1980; *Downs et al*., 1982; *Simpson et al*., 1993] are on average ~10 km wide (0.16° in longitude) and ~120 km high (2.0° in latitude), an area of ~1200 km^2 [see *Downs et al*., 1982]. The vertical uncertainty in the radar altimetry for the 1978 and 1980 oppositions ranges from 50 to 280 m (for individual points in Chryse and Amazonis Planitia) with an average of ~160 m [see *Downs et al*., 1982, Table 1]. Although these data are not sufficient to resolve the lobate scarps on Mars, the radar altimetry does resolve the large-scale, long-wavelength topographic variations in the highlands associated with the lobate scarps.

2.3. Photoclinometry

Photoclinometry utilizes a function that describes the photometric properties of the surface to recover the slope and the relative elevation between adjacent pixels of a digital image [*Wildey*, 1975; *Howard et al*., 1982; *Davis and Soderblom*, 1984; *McEwen*, 1991]. Photoclinometry is useful in obtaining short-wavelength topographic data for relatively small landforms with gentle slopes because the spatial resolution of the extracted topography is only limited by the spatial resolution of the image and because the method is sensitive to small changes in slope [*Davis and Soderblom*, 1984; *Tanaka and Davis*, 1988; *Watters and Robinson*, 1997]. We used the Minnaert photometric function because it is well suited for the surface of Mars [*Binder and Jones*, 1972; *Thorpe*, 1973; *Davis and Soderblom*, 1984; *Tanaka and Davis*, 1988; *McEwen*, 1991].

Critical parameters in the asymmetric photoclinometric method used here are the scattered light value (SLV) (sometimes referred to as the haze value) that corrects for light scattered in the atmosphere and from surfaces outside the pixel area and the horizontal digital number (HDN) (sometimes referred to as the flat field value) that represents the brightness value of a horizontal surface in an image [*Davis and Soderblom*, 1984; *Tanaka and Davis*, 1988]. The SLV is chosen by finding the brightness values of resolved shadows in the image. The HDN is selected through photointerpretation and is thus subjective. A more complete discussion of the SLV and HDN parameters and errors that result from their misestimations is given by *Watters and Robinson* [1997]. An independent check on the accuracy of photoclinometric elevations can be made by comparing them to elevations obtained by shadow measurements. In a study of graben in Syria Planum, *Tanaka and Davis* [1988] found that photoclinometrically derived elevations are within 10–15% of elevations determined by shadow measurements. *Mouginis-Mark and Robinson* [1992] also found good agreement between elevations derived from shadow measurements and photoclinometry in their study of the Olympus Mons caldera.

3. Results

3.1. Topography

Elevation profiles across seven moderate-scale scarps in northern Terra Cimmeria and the large-scale scarp Amenthes Rupes were obtained using photoclinometry. Profile lengths were selected to be the minimum necessary to span the full width of the lobate scarp in order to reduce uncertainties introduced by albedo variations and image calibration errors that scale with profile length. The SLV was chosen by examining pixels in prominent shadows cast by the walls of impact craters near the scarps. The HDN was determined by taking the average of a 9 × 9 array (81 pixels) of pixels located near the profile endpoints where the surface was judged to be roughly horizontal. An array of pixels is used in order to increase the signal-to-noise ratio (averaging reduces the effects of random and digitization noise and round off errors in calibration files). Our analysis of photoclinometric profiles across lobate scarps in northern Terra Cimmeria reveals that a variation of ±2 of the estimated HDN (which ranges from 775 to 923) does not significantly change the shape of the profiles or result in a change in the direction of slope of the scarp face (Figure 4). Gently sloping surfaces are, however, the most sensitive to small variations in HDN [*Davis and Soderblom*, 1984; *Watters and Robinson*, 1997].

Photoclinometric results for scarps studied in northern Terra Cimmeria (Figure 4) indicate that the measured relief ranges from 112 ± 9 m to 315 ± 24 m (error estimates on measured relief are based on a confidence in the derived elevations of ±7.5% [see *Tanaka and Davis*, 1988]). Although the photoclinometric profiles were located in an effort to measure the maximum relief on the lobate scarps, this may not have been achieved in every case. The topographic data indicate that lobate scarps have a simple morphology consisting of a steeply sloping scarp face and a gently sloping back scarp (Figures 4 and 5). Most of the scarp faces occur on the SW side of the structures. This suggests that fault planes dip to the NE, toward the boundary (Figure 5). The maximum slope on the scarp faces ranges from ~3° to 9° (Table 1).

MOLA data track 36 crosses northern Terra Cimmeria near the lobate scarps analyzed using photoclinometry and also crosses a moderate-scale, north-northwest trending lobate scarp located to the south (Figure 1). This scarp has a measured relief of about 327 ± 1 m (where the profile crosses it) (Figure 6), consistent with the range of relief determined for other moderate-scale lobate scarps in the region studied using photoclinometry (Table 1). The morphology of this lobate scarp, as reflected by the MOLA data, is also consistent with lobate scarps studied using photoclinometry. The maximum slope of the scarp face is ~4°, within the range of other moderate-scale lobate scarps studied. Like the other moderate-scale scarps in the region, the slope face is on the SW side of the structure. Unfortunately, a direct comparison of colocated photoclinometric profiles was not possible because a suitable Viking Orbiter image could not be found.

Data from MOLA track 36 (trending roughly N-S) indicate that the long-wavelength topography near the lobate scarps studied using photoclinometry (Figure 3) is relatively flat (Figure 7). Earth-based radar altimetry profiles (trending E-W) that cross northern Terra Cimmeria also indicate the topogra-

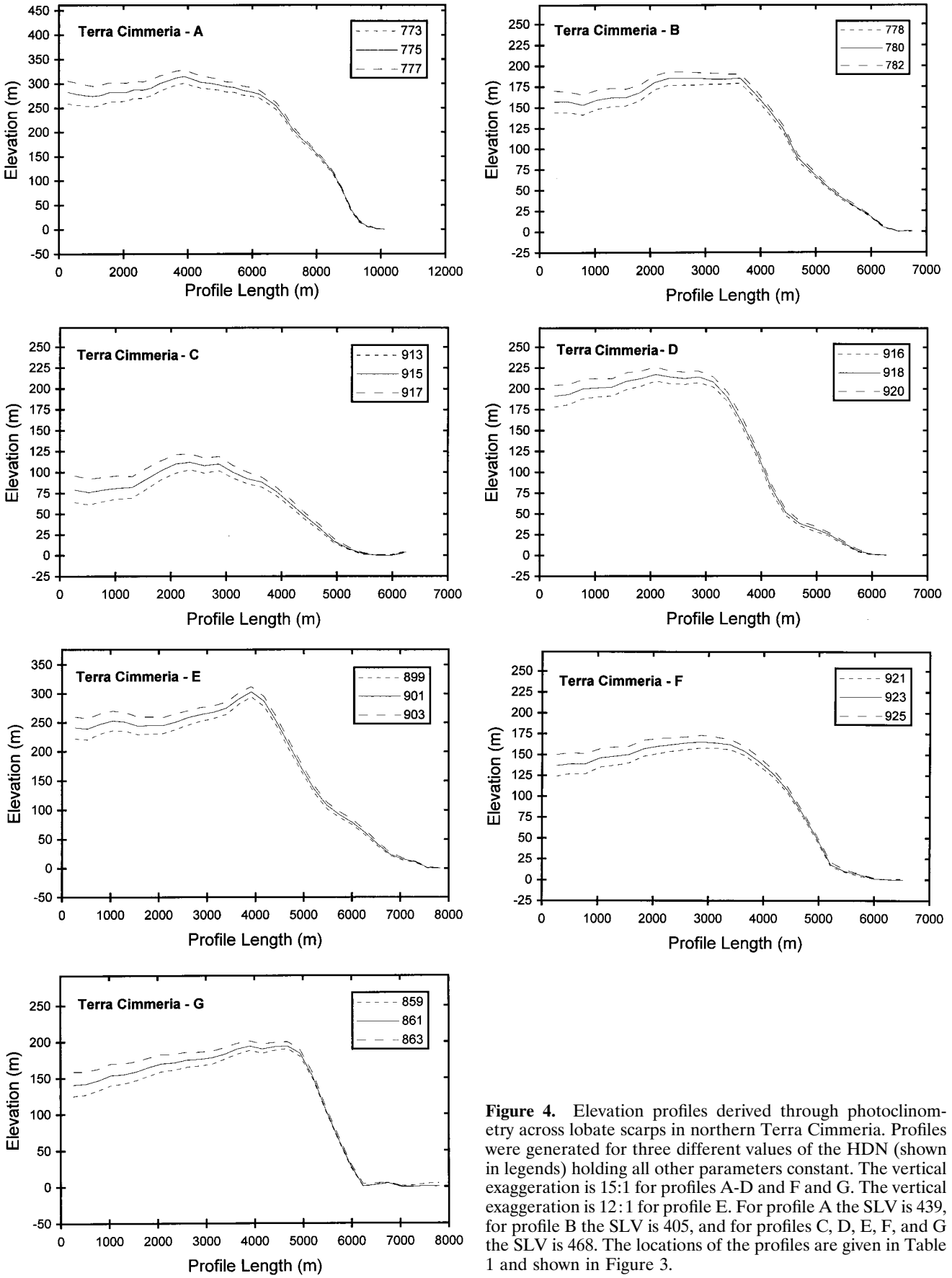

Figure 4. Elevation profiles derived through photoclinometry across lobate scarps in northern Terra Cimmeria. Profiles were generated for three different values of the HDN (shown in legends) holding all other parameters constant. The vertical exaggeration is 15:1 for profiles A-D and F and G. The vertical exaggeration is 12:1 for profile E. For profile A the SLV is 439, for profile B the SLV is 405, and for profiles C, D, E, F, and G the SLV is 468. The locations of the profiles are given in Table 1 and shown in Figure 3.

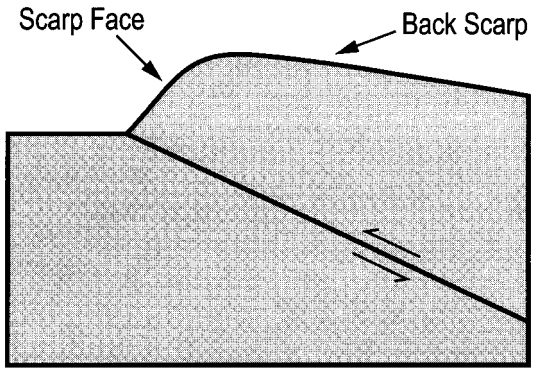

Figure 5. Schematic cross-sectional view of a lobate scarp. Lobate scarps consist of two morphologic features, a steeply sloping scarp face and a gently sloping back scarp. The proposed kinematic model for the formation of lobate scarps involves deformation over a buried thrust fault that propagates upward and eventually breaks the surface.

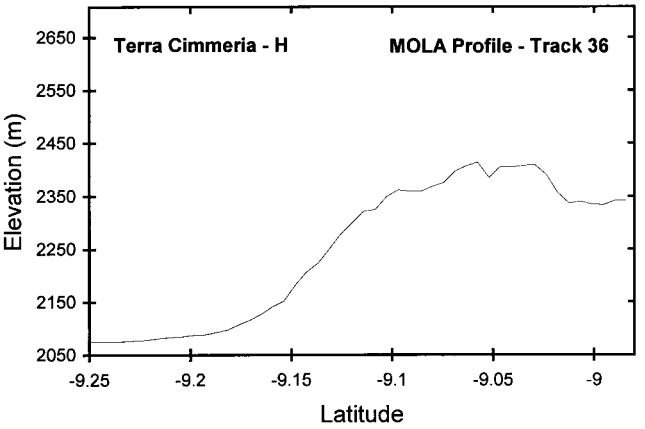

Figure 6. Mars Orbiter Laser Altimeter profile across a lobate scarp in northern Terra Cimmeria. The approximate location of the profile is shown in Figure 1. Data was extracted from track 36 located at ~234°W longitude [*NASA*, 1998]. Elevations are relative to a reference potential surface, and the vertical exaggeration is 15:1.

phy is relatively flat and gently sloping (Figure 8). The lobate scarp crossed by MOLA track 36 is about 1 km higher in elevation than the other lobate scarps in region (Figure 7). The regional slope of the long-wavelength topography in both the MOLA and the Earth-based radar altimetry data is toward the dichotomy (Figures 7 and 8).

Amenthes Rupes is over 400 km long with a measured relief of 1225 ± 92 m and a maximum slope of ~17° (Figure 9). It is comparable in scale to the Discovery Rupes on Mercury [*Watters et al*., 1998]. The scarp face of Amenthes Rupes, like the moderate-scale scarps of northern Terra Cimmeria, is on the SW side of the structure, distal to the scarp that marks the dichotomy boundary. Again, this suggests the fault plane dips to the NE, toward the dichotomy boundary. Earth-based radar altimetry profiles across Amenthes (trending E-W) indicate that the scarp is superposed on a gentle westward regional slope (~0.2°), away from the dichotomy (Figure 10) [also see *Smith and Zuber*, 1996].

3.2. Estimates of Horizontal Shortening and Displacement

To estimate horizontal shortening across Martian lobate scarps, we use a kinematic model that involves thrust faults that propagate upward and break the surface (Figure 5). The amount of horizontal shortening is estimated by assuming that it is a function of the dip of the fault plane and the displacement on the fault. The two variables in estimating the shortening in this way are the relief of the lobate scarp (h) and the fault plane dip (θ). The displacement (D) necessary to restore the topography to a planar surface is given by $D = h/\sin\theta$, and the horizontal shortening (S) is given by $S = h/\tan\theta$. Of the two variables, the most significant error in estimating the horizontal shortening is from the uncertainty in the fault plane dip.

Faulting occurs at fault plane dips (θ) for which the tectonic stress is a minimum. This minimum occurs when $\tan 2\theta = 1/\mu_s$,

Table 1. Lobate Scarp Dimensions and Estimates of Shortening and Displacement

Index	Viking Image	Resolution, m/pixel	Latitude	Longitude	Relief, m	Slope	S Range, m	S $\theta = 25°$, m	D $\theta = 25°$, m
				Terra Cimmeria					
A	629A21	260	5.7° S	237.2°W	315 ± 24	7°	450–866	676 ± 51	745 ± 56
B	629A21	260	5.4° S	236.6°W	185 ± 14	5°	264–508	397 ± 30	438 ± 33
C	629A22	261	6.0° S	234.0°W	112 ± 9	3°	160–308	240 ± 17	265 ± 20
D	629A22	261	4.2° S	235.4°W	217 ± 16	8°	310–596	465 ± 35	514 ± 39
E	629A22	261	3.2° S	237.2°W	303 ± 23	8°	433–833	650 ± 49	717 ± 54
F	629A22	261	5.3° S	234.2°W	165 ± 12	6°	236–453	354 ± 27	390 ± 29
G	629A22	261	5.8° S	235.5°W	194 ± 15	9°	277–533	416 ± 31	459 ± 34
H	···	···	9.4° S	235.4°W	327 ± 1	4°	467–898	701 ± 2	774 ± 2
				Amenthes Rupes					
	379S46	243	1.5° N	249.5°W	1225 ± 92	17°	1750–3366	2627 ± 197	2899 ± 217

The relief of lobate scarps A–G and Amenthes Rupes was determined using photoclinometry, and the relief of lobate scarp H was determined with MOLA data. It should be noted that photoclinometric profiles were located in an effort to measure the maximum relief on the lobate scarps; however, this may not have been achieved in every case. Also, the relief of the lobate scarp measured using MOLA data is the maximum relief where the track crosses the structure. Error estimates on the measured relief, shortening ($\theta = 25°$), and displacement ($\theta = 25°$) for lobate scarps A–G and Amenthes Rupes are based on a confidence in the photoclinometrically derived elevations of ±7.5% [see *Tanaka and Davis*, 1988]. The shortening range for these scarps is based on the measured relief in the derived elevations for a range in HDN of ±2 at $\theta = 20°$ and 35°. For scarp H the estimated error on the measured relief and shortening is based on a precision of the MOLA data of ±1 m [see *Smith et al*., 1998], and the range in shortening is based on the measured relief for $\theta = 20°$ and 35°. The location of profiles A–G are shown in Figure 3 and the location of profile H is shown in Figure 1.

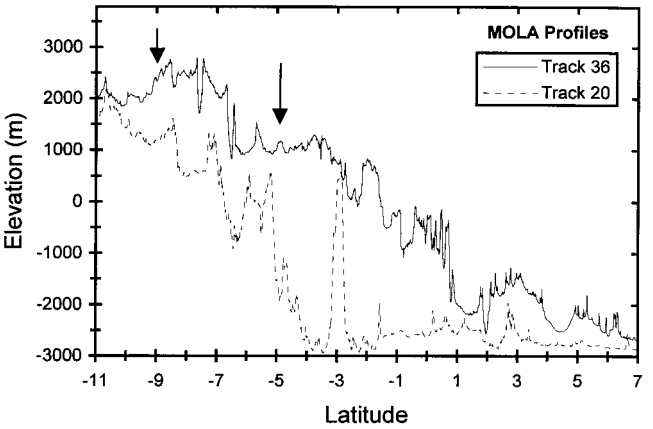

Figure 7. Mars Orbiter Laser Altimeter profiles across the dichotomy in northern Terra Cimmeria. More than 2.5 km of relief is indicated over the transition from the heavily cratered highlands to the lowlands. The approximate locations of the profiles are shown in Figure 1. Data were extracted from tracks 36 and 20 located at ~234°W and ~227°W longitude, respectively [*NASA*, 1998]. The long arrow indicates the approximate location of lobate scarps A–G (Table 1 and Figure 3), and the short arrow indicates the location of lobate scarp H (Table 1 and Figure 1). Elevations are relative to a reference potential surface, and the vertical exaggeration is 100:1.

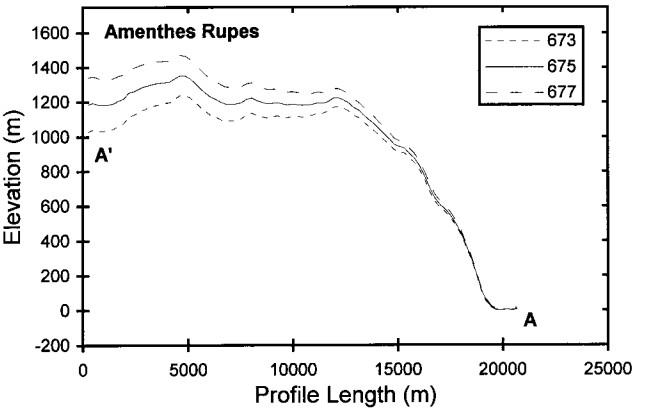

Figure 9. Elevation profiles derived through photoclinometry across Amenthes Rupes. Profiles were generated for three different values of the HDN (shown in legend) holding all other parameters constant (Viking Orbiter image 379S46, image resolution 243 m/pixel). The SLV is 436. The location of the profiles is shown in Figure 2. Vertical exaggeration is 8:1.

where μ_s, by analog with ordinary sliding friction, is defined as the coefficient of internal friction [see *Jaeger and Cook*, 1979; *Turcotte and Schubert*, 1982]. Data obtained from laboratory experiments on the maximum shear stress to initiate sliding as a function of normal stress, for a variety of rock types, are best fit by a maximum coefficient of static friction of 0.6 to 0.9 (best fit $\mu_s = 0.85$) [*Byerlee*, 1978]. These data suggest that thrust faults will form with dips ranging from ~24° to 30°, ~25° for $\mu_s = 0.85$. This theoretical range of fault plane dips is in good agreement with field measurements of θ for terrestrial thrust faults that typically range between 20° and 25° [see *Jaeger and Cook*, 1979]. A notable exception is the large-scale Wind River thrust fault with a average θ of 35° that extends to a depth of 36 km [*Brewer et al.*, 1980]. In this analysis we therefore conservatively assume that the thrust faults associated with lobate scarps will fall within a range in θ of 20° to 35° and that the optimum θ is 25°.

It is also assumed, in the absence of any data to the contrary, that fault plane dips are uniform (i.e., linear, not curved). This assumption is reasonable because there are terrestrial thrust faults with uniform fault plane dips that do not significantly steepen or shallow with depth. The Wind River thrust [*Brewer et al.*, 1980] and other thrust faults that cut the Precambrian basement of the Rocky Mountain Foreland in Wyoming [*Gries*, 1983; *Stone*, 1985] are examples. Some thrust faults in this region exhibit consistent fault plane dip angles in the Precam-

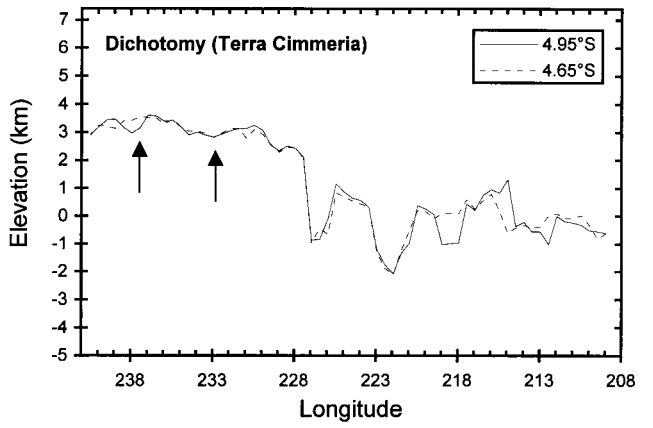

Figure 8. Goldstone Earth-based radar altimetry profiles across northern Terra Cimmeria and the crustal dichotomy. The latitudes of the profiles are given in the legend, and the approximate locations of the western halves of the profiles are shown in Figure 1. The arrows indicate the approximate location of the lobate scarps A–G (Table 1 and Figure 3). Altimetry is relative to the 6.1 mbar surface which is offset to the MOLA data reference potential surface by approximately −1600 m on average [*Smith and Zuber*, 1998]. The vertical exaggeration is 100:1.

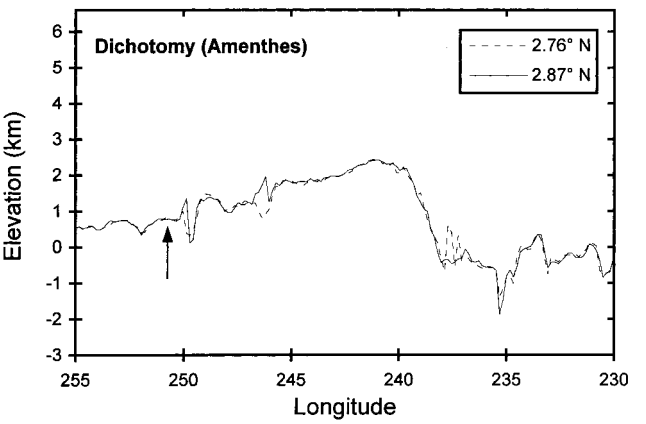

Figure 10. Goldstone Earth-based radar altimetry profiles across the crustal dichotomy in the Amenthes region. The arrow indicates the approximate location of Amenthes Rupes shown in Figure 2. The latitude of the profiles are given in the legend and their approximate locations are shown in Figure 1. Altimetry is relative to the 6.1 mbar surface which is offset to the MOLA data reference potential surface by approximately −1600 m on average [*Smith and Zuber*, 1998]. The vertical exaggeration is 100:1.

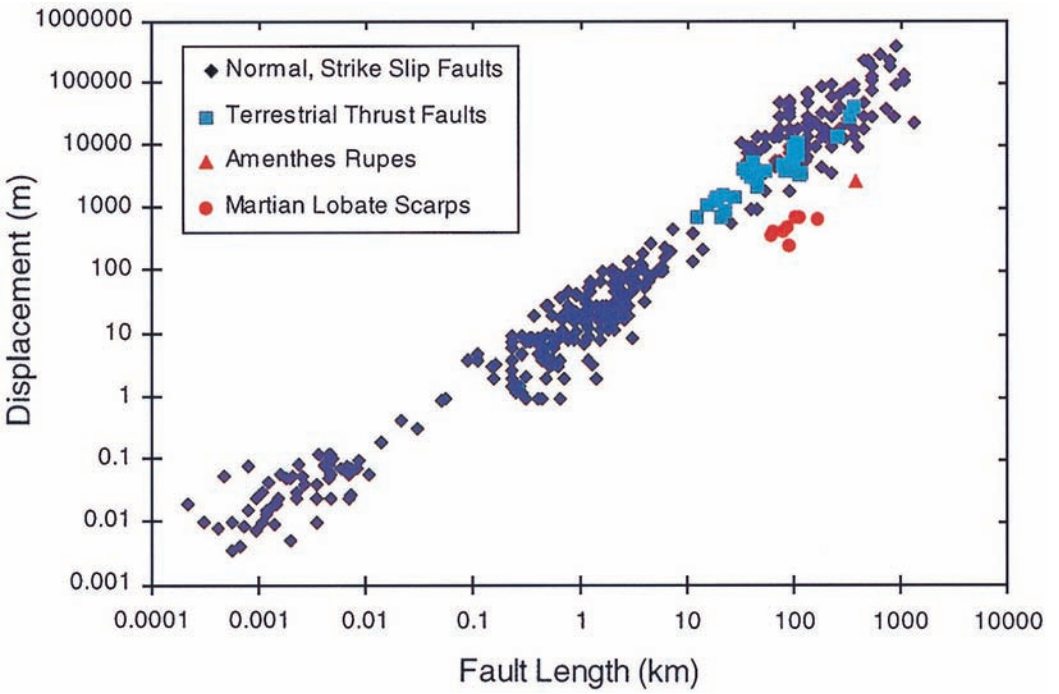

Plate 1. A log-log plot of maximum displacement as a function of fault length for terrestrial faults and thrust faults, Amenthes Rupes, and eight other Martian lobate scarps (see legend). The data for terrestrial faults are from nine different data sets (includes data for 29 thrust faults) [see *Cowie and Scholz*, 1992].

brian basement that steepen upward only where they cut Paleozoic sedimentary sequences [*Stone*, 1985]. The dips on the thrust faults cited, excluding the Wind River thrust, cut the Precambrian basement at angles between 25° and 30°.

From our new topographic data and the assumptions outlined above, the horizontal shortening was estimated using the measured h of the lobate scarps and a range in θ (20° to 35°). Our results for the moderate-scale scarps of northern Terra Cimmeria indicate that the amount of shortening ranges from a few hundred meters to just under a kilometer (Table 1), with an average of ~490 m at $\theta = 25°$ ($n = 8$). The bulk horizontal shortening across the lobate scarp belt shown in Figure 3 is estimated to be roughly 2.0 to 2.9 km (based on traverses through the highlands that intersect four to six scarps and assuming an average shortening of 490 m per scarp). The amount of horizontal shortening across Amenthes Rupes is of the order of 1.8 to 3.4 km (~2.6 km at $\theta = 25°$) (see Table 1). Thus the shortening across the moderate-scale lobate scarps in northern Terra Cimmeria (shown in Figure 3) is roughly comparable to the shortening across Amenthes Rupes, suggesting that a similar bulk compressional strain was generated across the region by the deformation event. It should be noted that the estimates given above assume that overthrusting (where the fault block is translated over the fault ramp onto the flat) is not a significant component of the total horizontal shortening. This assumption is supported through observations that no significant offsets occur in crater rims crosscut by scarps. If overthrusting is significant, our estimates of horizontal shortening may be only lower limits.

3.3. Comparison With Terrestrial Faults

There is growing evidence based on field observations of terrestrial faults that indicates that a positive correlation exists between the maximum displacement on a fault (D) and the length of the fault trace (L) [*Cowie and Scholz*, 1992; *Gillespie et al*., 1992; *Dawers et al*., 1993; *Cartwright et al*., 1995]. This relationship also seems to hold for planetary faults [*Schultz*, 1995; *Schultz and Fori*, 1996; *Schultz*, 1997; *Watters et al*., 1997, 1998, 1999]. The exact nature of the relationship between D and L is still being debated. *Cowie and Scholz* [1992] suggest that the D-L relationship for continental faults is linear such that $D = \gamma L$ and γ is determined by rock type and tectonic setting (Plate 1). It has also been suggested that there is a power law relationship $D = cL^n$,, where c is a constant related to material properties with n ranging from 1 to 2 [see *Gillespie et al*., 1992]. Regardless of its exact nature, a consistent scaling relationship between D and L holds for all the fault types (i.e., normal, strike-slip, and thrust) in a wide variety of tectonic settings and a wide range of length scales [*Cowie and Scholz*, 1992]. The ratio of displacement to fault length (γ) ranges between 10^0 and 10^{-3} for terrestrial faults [*Cowie and Scholz*, 1992]. Some of the scatter in the D and L data probably reflects the growth of faults by segment linkage where the scaling characteristics change at different stages of fault evolution [*Cartwright et al*., 1995, 1996; *Dawers and Anders*, 1995; *Wojtal*, 1996; *Moore and Schultz*, 1999].

The value of γ for the Martian lobate scarps (obtained by a linear fit to D-L data with estimates of D based on $\theta = 25°$) is 6.2×10^{-3} ($n = 9$) (Plate 1). This is consistent with the values of γ of terrestrial fault populations [see *Cowie and Scholz*, 1992]. The displacements on the faults associated with lobate scarps are about an order of magnitude lower than terrestrial thrust faults (Plate 1); however, they fall within the same range determined for Mercurian lobate scarps [*Watters et al*., 1998, 1999]. This is likely a reflection of the difference in tectonic setting. Most terrestrial thrust faults occur in foreland fold and thrust belts located at convergent plate margins, as is the case for the thrust faults plotted in Plate 1 that occur in the foreland thrust belt of the Canadian Rocky Mountains [*Elliott*, 1976a, b].

3.4. Estimates of Compressional Strain

The compressional strain reflected by the lobate scarps in the northern Terra Cimmeria–Amenthes region can be estimated using the displacement-length scaling relationship for these structures. If the D-L scaling relationship of a fault population is known, the strain can be calculated using fault lengths alone [*Scholz and Cowie*, 1990; *Cowie et al*., 1993]. The strain for large faults ($L \geq$ the maximum depth of faulting) is given by

$$\varepsilon = \frac{\cos(\theta)}{A} \sum_{k=1}^{n} D_k L_k \qquad (1)$$

where θ is the fault plane dip, A is the size of the survey area, n is the total number of faults, and $D = \gamma L$ [*Cowie et al*., 1993]. The value of γ for the lobate scarps studied here ($n = 9$), obtained by a linear fit to the D-L data with estimates of D based on $\theta = 25°$, is 6.2×10^{-3}. The lengths of lobate scarps ($n = 23$) were measured in the heavily cratered highlands (Npld) in the northern Terra Cimmeria–Amenthes region, adjacent to the crustal dichotomy boundary (from 225°W to 255°W). The compressional strain in the heavily cratered highlands is estimated to be between 0.175% and 0.153% for a range in θ of 20° to 35° (0.169% for $\theta = 25°$).

4. Discussion

4.1. Origin of the Crustal Dichotomy

The origin of the dichotomy that divides the heavily cratered highlands in the southern hemisphere from the younger, lightly cratered lowlands of the northern hemisphere is one of the most important unresolved questions about the geologic evolution of Mars. Although it is generally agreed that the dichotomy is a geologic boundary, *Smith and Zuber* [1996] argue that the apparent topographic difference between the northern and southern hemisphere reflects a center of mass–center of figure offset and that there is no clear topographic depression in the northern hemisphere. It is difficult to reconcile this interpretation with the topographic data from Earth-based radar altimetry and from MOLA [see *Smith et al*., 1998, Figure 1; *Frey et al*., 1998]. Earth-based radar altimetry profiles that cross the boundary in Amenthes (Figure 10) and northern Terra Cimmeria (Figure 8) show an average elevation change of ~2.5 km. Initial results from MOLA confirm these measurements (Figure 7) and show that the regional elevation change is >2.5 km and up to 6 km in some areas [*Frey et al*., 1998; *Smith et al*., 1998]. Thus in the northern Terra Cimmeria–Amenthes region, and elsewhere along the dichotomy, the northern plains are significantly lower than the highlands, and the dichotomy is a real and distinct topographic feature [*Watters and Robinson*, 1998; *Frey et al*., 1998].

A variety of models have been proposed for the origin of the crustal dichotomy. These models fall into two groups, one involving impact processes and the other involving internal or endogenic processes. Impact models involve either one giant impact [*Wilhelms and Squyres*, 1984; *McGill*, 1989] or multiple impacts [*Frey and Schultz*, 1988]. These models require that the dichotomy is very old (early or pre-Noachian), forming before the end of the period of heavy bombardment. *McGill and Dimitriou* [1990] cite late Noachian to early Hesperian fracturing and faulting in the northern lowlands and along the dichotomy boundary as evidence of a younger age of formation. They propose that the early northern crust was thinned and subsided through delamination or crustal erosion by mantle convection. The eroded crustal material is thought to have been globally dispersed [*McGill and Dimitriou*, 1990].

There is evidence of fracturing and faulting along the boundary in Amenthes and northern Terra Cimmeria (Figure 1). The presence of lobate scarps in proximity to and oriented parallel with the boundary suggests that the dichotomy in this region has a distinct tectonic signature. The age of the lobate scarps is difficult to determine through crater counts because the structures are relatively small in areal extent. However, a number of scarps crosscut the walls and floors of large (>16 km diameter) degraded impact craters, while smaller (<16 km diameter), relatively fresh craters are superimposed on some of the scarps. On the basis of crater ages and crosscutting relationships, *Maxwell and McGill* [1988] suggest that scarp formation in the highlands of Amenthes near the dichotomy boundary occurred during the late Noachian. The fact that some of the lobate scarps in northern Terra Cimmeria deform intercrater plains estimated to be early Hesperian in age [*Greeley and Guest*, 1987] suggests that the formation of the scarps may have continued into the early Hesperian. *Wilhelms and Baldwin* [1989] conclude that wrinkle ridges and scarps in this region formed in the early Hesperian. Thus it is plausible that the formation of the fractures and faults associated with the dichotomy and the formation of the lobate scarps were roughly syntectonic, separated spatially by ~400 km, if the boundary has always been close to its present position, as suggested by *McGill and Dimitriou* [1990]. Models proposing that only lithospheric extension accompanied the formation of the crustal dichotomy [e.g., *McGill and Dimitriou*, 1990] cannot account for the observed compressional deformation.

4.2. Plate Tectonics

A plate tectonic model has been proposed for the origin of the dichotomy where ancient crust was removed through hemispheric subduction and the dichotomy boundary marks relic plate margins [*Sleep*, 1994]. Hemispheric subduction may be a viable hypothesis for the origin of the crustal dichotomy because it is the dominant process for crustal thinning on the Earth [*Turcotte*, 1996], and it is consistent with the remarkably flat topography of the northern plains revealed by the MOLA data [*Turcotte*, 1999]. In his model, *Sleep* [1994] suggests that the dichotomy boundary extending from the Tyrrhena region, through Amenthes and Cimmeria, to Memnonia is a passive margin. *Watters and Robinson* [1998] suggest that compressional stresses due to flexure from an emerging spreading ridge and ambient compressional stresses caused by subsequent rapid spreading are one possible mechanism to account for the formation of the lobate scarps and the fractures along the dichotomy boundary in Amenthes and northern Terra Cimmeria. This model also suggests that the boundary in the northern Terra Cimmeria–Amenthes region is a passive margin. The analogy between the dichotomy boundary and passive margins is further strengthened by MOLA data. *Frey et al*. [1998] report that the regional topography of the dichotomy boundary zone indicated in the MOLA data (a 2 to 4 km step between two nearly flat surfaces over a distance of few hundred kilometers) is consistent with some terrestrial passive margins.

There are, however, challenges to applying a plate tectonic model to Mars. *Pruis and Tanaka* [1995] question many aspects of the model proposed by *Sleep* [1994]. They argue that evidence of tectonism and volcanism in areas predicted by the

Sleep [1994] model is sparse and that some structures that seem to agree with the model often have incorrect orientations or modes of origin. New topographic data, images, and magnetic and gravity field measurements being returned from the Mars Global Surveyor will allow an in-depth evaluation of the possible role of plate tectonics in Martian geologic history.

5. Conclusions

An analysis of lobate scarps in the northern Terra Cimmeria–Amenthes region using new topographic data indicates that they reflect significant compressional deformation of the heavily cratered highlands near the dichotomy boundary. Crustal shortening due to thrust faulting is of the order of 2 to 3 km locally, and the regional compressional strain in the highlands (Npld) adjacent to the dichotomy boundary is ~0.17%. The *D*-*L* relationships of the lobate scarps studied ($\gamma = 6.2 \times 10^{-3}$) is comparable to those observed for terrestrial faults (γ ranging from 10^{0} to 10^{-3}). The formation of fractures along the boundary appears to be roughly syntectonic with the formation of the thrust faults responsible for the lobate scarps. These new data and observations are consistent with a tectonic origin for the dichotomy, involving both extensional and compressional deformation. A successful model for the origin of the crustal dichotomy must account for its distinct topographic and tectonic signature. It must also explain the presence of both the lobate scarps (compressional deformation) and fractures (extensional deformation) associated with the dichotomy boundary.

Acknowledgments. We thank Kenneth L. Tanaka and Craig R. Bina for their helpful reviews of the manuscript. We also thank Norman H. Sleep for helpful discussions about the possibility of plate tectonics on Mars. The PICS software used to acquire the photoclinometric data was provided by the USGS Flagstaff. This research was supported by grants from National Aeronautics and Space Administration's Planetary Geology and Geophysics Program and the Mars Data Analysis Program.

References

Binder, A. B., and J. C. Jones, Spectrophotometric studies of the photometric function, composition, and distribution of the surface materials of Mars, *J. Geophys. Res*., *77*, 3005–3020, 1972.

Brewer, J. A., S. B. Smithson, J. E. Oliver, S. Kaufman, and L. D. Brown, The Laramide orogeny: Evidence form COCORP deep crustal seismic profiles in the Wind River mountains, Wyoming, *Tectonophysics*, *62*, 165–189, 1980.

Byerlee, J., Friction of rocks, *Pure Appl. Geophys*., *116*, 615–626, 1978.

Cartwright, J. A., B. D. Trudgill, and C. S. Mansfield, Fault growth by segment linkage: An explanation for scatter in maximum displacement and trace length data from the Canyonlands Grabens of SE Utah, *J. Struct. Geol*., *17*, 1319–1326, 1995.

Cartwright, J. A., C. S. Mansfield, and B. D. Trudgill, The growth of normal faults by segment linkage, in *Modern Developments in Structural Interpretation: Validation and Modelling*, edited by P. G. Buchanan and D. A. Nieuwland, *Geol. Soc. Spec. Publ*., *99*, 163–177, 1996.

Cordell, B. M., and R. G. Strom, Global tectonics of Mercury and the Moon, *Phys. Earth Planet. Inter*., *15*, 146–155, 1977.

Cowie, P. A., and C. H. Scholz, Displacement-length scaling relationship for faults: Data synthesis and discussion, *J. Struct. Geol*., *14*, 1149–1156, 1992.

Cowie, P. A., C. H. Scholz, M. Edwards, and A. Malinverno, Fault strain and seismic coupling on mid-ocean ridges, *J. Geophys. Res*., *98*, 17911–17920, 1993.

Davis, P. A., and L. A. Soderblom, Modeling crater topography and albedo from monoscopic Viking Orbiter images, *J. Geophys. Res*., *89*, 9449–9457, 1984.

Dawers, N. H., and M. H. Anders, Displacement-length scaling and fault linkage, *J. Struct. Geol*., *17*, 607–614, 1995.

Dawers, N. H., Anders, M. H., and Scholz, C. H., Growth of normal faults: Displacement-length scaling, *Geology*, *21*, 1107–1110, 1993.

Downs, G. S., P. J. Mouginis-Mark, S. H. Zisk, and T. W. Thompson, New radar derived topography for the northern hemisphere of Mars, *J. Geophys. Res*., *87*, 9747–9754, 1982.

Elliott, D., The energy balance and deformation mechanisms of thrust sheets, *Philos. Trans. R. Soc. London, on Ser. A*, *283*, 289–312, 1976a.

Elliott, D., The motion of thrust sheets, *J. Geophys. Res*., *81*, 949–963, 1976b.

Frey, H., and R. A. Schultz, Large impact basins and the mega-impact origin for the crustal dichotomy on Mars, *Geophys. Res. Lett*., *15*, 229–232, 1988.

Frey, H., S. E. Sakimoto, and J. Roark, The MOLA topographic signature at the crustal dichotomy boundary zone on Mars, *Geophys. Res. Lett*., *25*, 4409–4412, 1998.

Gillespie, P. A., J. J. Walsh, and J. Watterson, Limitations of dimension and displacement data from single faults and the consequences for data analysis and interpretation, *J. Struct. Geol*., *14*, 1157–1172, 1992.

Greeley, R., and J. E. Guest, Geologic map of the eastern equatorial region of Mars, scale 1:15,000,000, *U.S. Geol. Surv. Misc. Invest. Ser. Map*, *I-1802-B*, 1987.

Gries, R., Oil and gas prospecting beneath Precambrian of foreland thrust plates in Rocky Mountains, *AAPG Bull*., *67*, 1–28, 1983.

Howard, A. D., K. R. Blasius, and J. A. Cutts, Photoclinometric determination of the topography of the martian north polar cap, *Icarus*, *50*, 245–258, 1982.

Jaeger, J. C., and N. G. W. Cook, *Fundamentals of Rock Mechanics*, 3rd ed., 593 pp., Chapman and Hall, New York, 1979.

Maxwell, T. A., and G. E. McGill, Ages of fracturing and resurfacing in the Amenthes Region, Mars, *Proc. Lunar Planet. Sci. Conf*., *18th*, 701–711, 1988.

McEwen, A. S., Photometric functions for photoclinometry and other applications, *Icarus*, *92*, 298–311, 1991.

McGill, G. E., Buried topography of Utopia, Mars: Persistence of a giant impact depression, *J. Geophys. Res*., *94*, 2753–2759, 1989.

McGill, G. E., and A. M. Dimitriou, Origin of the Martian global dichotomy by crustal thinning in the late Noachian or early Hesperian, *J. Geophys. Res*., *95*, 12595–12605, 1990.

Melosh, H. J., and W. B. McKinnon, The tectonics of Mercury, in *Mercury*, edited by F. Vilas, C. R. Chapman, and M. S. Matthews, pp. 374–400, Univ. of Ariz. Press, Tucson, 1988.

Moore, J. M., and R. A. Schultz, Processes of Faulting in Jointed Rocks of Canyonlands National Park, Utah, *Geol. Soc. Am. Bull*., *111*, 808–822, 1999.

Mouginis-Mark, P. J., and M. S. Robinson, Evolution of the Olympus Mons caldera, Mars, *Bull. Volcanol*., *54*, 347–360, 1992.

NASA, Mission to Mars: Digital image map [CD-ROM], USA_NASA_PDS_VO_2004, NASA Planet. Data Syst., Pasadena, Calif., 1991.

NASA, Mission to Mars: Mars Global Surveyor [CD-ROM], USA_NASA_PDS_MGS_0001, NASA Planet. Data Syst., Pasadena, Calif., 1998.

Pruis, M. J., and K. L. Tanaka, The Martian northern plains did not result from plate tectonics (abstract), *Lunar Planet. Sci. Conf*., *XXVI*, 1147–1148, 1995.

Roth, L. E., G. S. Downs, and R. S. Saunders, Radar altimetry of south Tharsis, Mars, *Icarus*, *42*, 287–316, 1980.

Scholz, C. H., and P. A. Cowie, Determination of geologic strain from fault slip data, *Nature*, *346*, 837–839, 1990.

Schultz, R. A., Gradients in extension and strain at Valles Marineris, Mars, *Planet. Space Sci*., *43*, 1561–1566, 1995.

Schultz, R. A., Displacement-length scaling for terrestrial and Martian faults: Implications for Valles Marineris and shallow planetary grabens, *J. Geophys. Res*., *102*, 12009–12015, 1997.

Schultz, R. A., and A. N. Fori, Fault-length statistics and implications of graben sets at Candor Mensa, Mars, *J. Struct. Geol*., *18*, 373–383, 1996.

Simpson, R. A., J. K. Harmon, S. H. Zisk, T. W. Thompson, and D. O. Muhleman, Radar determination of Mars surface properties, in *Mars*, edited by H. Kieffer et al., pp. 652–685, Univ. of Ariz. Press, Tucson, 1993.

Sleep, N. H., Martian plate tectonics, *J. Geophys. Res*., *99*, 5639–5656, 1994.

Smith, D. E., and M. T. Zuber, The shape of Mars and the topographic signature of the hemispheric dichotomy, *Science*, *271*, 184–188, 1996.

Smith, D. E., and M. T. Zuber, The relationship between MOLA northern hemisphere topography and the 6.1-Mbar atmospheric pressure surface of Mars, *Geophys. Res. Lett*., *25*, 4397–4400, 1998.

Smith, D. E., et al., Topography of the northern hemisphere of Mars from the Mars Orbiter Laser Altimeter, *Science*, *279*, 1686–1692, 1998.

Stone, D. S., Geologic interpretation of seismic profiles, Big Horn Basin, Wyoming, I, East flank, in *Seismic Exploration of the Rocky Mountain Region*, edited by R. R. Gries and R. C. Dyer, pp. 165–174, Rocky M. Assoc. of Geol., Denver, Colo., 1985.

Strom, R. G., N. J. Trask, and J. E. Guest, Tectonism and volcanism on Mercury, *J. Geophys. Res*., *80*, 2478–2507, 1975.

Tanaka, K. L., The stratigraphy of Mars, *Proc. Lunar Planet. Sci. Conf. 17th*, Part I, *J. Geophys. Res*., *91*, suppl., E139–E158, 1986.

Tanaka, K. L., and P. A. Davis, Tectonic history of the Syria Planum province of Mars, *J. Geophys. Res*., *93*, 14893–14907, 1988.

Thorpe, T. E., Mariner 9 photometric observations of Mars from November 1971 through March 1972, *Icarus*, *20*, 482–489, 1973.

Turcotte, D. L., Martian tectonics: Why the global dichotomy and the Tharsis Uplift (abstract), *Lunar Planet. Sci. Conf*., *XXVII*, 1345–1346, 1996.

Turcotte, D. L., Tectonics and volcanism on Mars: What do we and what don't we know? (abstract), *Lunar Planet. Sci. Conf*., *XXX*, 1187–1188, 1999.

Turcotte, D. L., and G. Schubert, *Geodynamics: Application of Continuum Physics to Geological Problems*, 450 pp., John Wiley, New York, 1982.

Watters, T. R., Compressional tectonism on Mars, *J. Geophys. Res*., *98*, 17049–17060, 1993.

Watters, T. R., and M. S. Robinson, Radar and photoclinometric studies of wrinkle ridges on Mars, *J. Geophys. Res*., *102*, 10889–10903, 1997.

Watters, T. R., and M. S. Robinson, Lobate Scarps and the origin of the crustal dichotomy on Mars (abstract), *Lunar Planet. Sci. Conf*., *XXIX*, 1475–1476, 1998.

Watters, T. R., M. S. Robinson, and A. C. Cook, Comparison of Discovery Rupes, Mercury with terrestrial thrust faults: New estimates of the decrease in radius of the planet due to global contraction (abstract), *Lunar Planet. Sci. Conf*., *XXVIII*, 1507–1508, 1997.

Watters, T. R., M. S. Robinson, and A. C. Cook, Topography of lobate scarps on Mercury: New constraints on the planet's contraction, *Geology*, *26*, 991–994, 1998.

Watters, T. R., M. S. Robinson, and R. A. Schultz, Comparative studies of displacement-length relations of lobate scarps on Mercury and Mars with terrestrial faults (abstract), *Lunar Planet. Sci. Conf*., *XXX*, 1826–1827, 1999.

Wichman, R. W., and P. H. Schultz, Sequence and mechanisms of deformation around the Hellas and Isidis Impact Basins on Mars, *J. Geophys. Res*., *94*, 17333–17357, 1989.

Wildey, R. L., Generalized photoclinometry of Mariner 9, *Icarus*, *25*, 613–626, 1975.

Wilhelms, D. E., and R. J. Baldwin, The role of igneous sills in shaping the Martian uplands, *Lunar Planet Sci*., *XIX*, 355–365, 1989.

Wilhelms, D. E., and S. W. Squyres, The martian hemispheric dichotomy may be due to a giant impact, *Nature*, *309*, 138–140, 1984.

Wojtal, S. F., Changes in fault displacement populations correlated to linkage between faults, *J. Struct. Geol*., *18*, 265–279, 1996.

Zuber, M. T., D. E. Smith, S. C. Solomon, D. O. Muhleman, J. W. Head, J. B. Garvin, J. B. Abshire, and J. L. Bufton, The Mars Observer Laser Altimeter investigation, *J. Geophys. Res*., *97*, 7781–7797, 1992.

Zuber, M. T., et al., Observations of the north polar region of Mars from the Mars Orbiter Laser Altimeter, *Science*, *282*, 2053–2060, 1998.

M. S. Robinson, Department of Geological Sciences, Northwestern University, Evanston, IL 60209.

T. R. Watters, Center for Earth and Planetary Studies, National Air and Space Museum, Smithsonian Institution, Washington, DC 20560. (twatters@ceps.nasm.edu)

(Received November 12, 1998; revised April 13, 1999; accepted April 15, 1999.)